

OPEN ACCESS

Complementary test of the dark matter self-interaction in dark U(1) model by direct and indirect dark matter detection

To cite this article: Chian-Shu Chen *et al*/JCAP01(2016)013

View the [article online](#) for updates and enhancements.

Related content

- [Probing dark matter self-interaction in the Sun with IceCube-PINGU](#)
Chian-Shu Chen, Fei-Fan Lee, Guey-Lin Lin *et al*.
- [Long-range Self-interacting Dark Matter in the Sun](#)
Jing Chen, Zheng-Liang Liang, Yue-Liang Wu *et al*.
- [Detecting boosted dark matter from the Sun with large volume neutrino detectors](#)
Joshua Berger, Yanou Cui and Yue Zhao

Recent citations

- [Exploring light mediators with low-threshold direct detection experiments](#)
Felix Kahlhoefer *et al*



Credit: ESO/M. Kornmesser



AMERICAN
ASTRONOMICAL
SOCIETY

IOP | ebooks™

Your first choice for astronomy, astrophysics,
solar physics, and planetary science ebooks.

Start exploring the collection—download the
first chapter of every title for free.

Complementary test of the dark matter self-interaction in dark U(1) model by direct and indirect dark matter detection

Chian-Shu Chen,^{a,c,d} Guey-Lin Lin^b and Yen-Hsun Lin^b

^aPhysics Division, National Center for Theoretical Sciences, No. 101, Section 2, Kuang-Fu Road, Hsinchu, Taiwan, 30010 R.O.C.

^bInstitute of Physics, National Chiao Tung University, 1001 University Road, Hsinchu, Taiwan, 300 R.O.C.

^cDepartment of Physics, National Tsing Hua University, No. 101, Section 2, Kuang-Fu Road, Hsinchu, Taiwan, 30010 R.O.C.

^dInstitute of Physics, Academia Sinica, 128 Sec. 2, Academia Rd., Nangang, Taipei, Taiwan, 11529 R.O.C.

E-mail: chianshu@gmail.com, glin@cc.nctu.edu.tw, chris.py99g@g2.nctu.edu.tw

Received June 4, 2015

Revised November 24, 2015

Accepted December 9, 2015

Published January 7, 2016

Abstract. The halo dark matter (DM) can be captured by the Sun if its final velocity after the collision with a nucleus in the Sun is less than the escape velocity. We consider a selfinteracting dark matter (SIDM) model where U(1) gauge symmetry is introduced to account for the DM self-interaction. Such a model naturally leads to isospin violating DM-nucleon interaction, although isospin symmetric interaction is still allowed as a special case. We present the IceCube-PINGU 2σ sensitivity to the parameter range of the above model with 5 years of search for neutrino signature from DM annihilation in the Sun. This indirect detection complements the direct detection by probing those SIDM parameter ranges which are either the region for very small m_χ or the region opened up due to isospin violations.

Keywords: neutrino experiments, dark matter theory, dark matter experiments

ArXiv ePrint: [1505.03781](https://arxiv.org/abs/1505.03781)



Contents

1	Introduction	1
2	Scattering via light mediator exchange	3
2.1	Scattering with vector mediator	4
2.2	Scattering with scalar mediator	5
3	DM accumulation in the Sun	6
3.1	The evolution equation	6
3.2	Numerical results	8
4	Testing SIDM model in IceCube-PINGU	10
4.1	Neutrino signal and the atmospheric background	10
4.2	The IceCube sensitivity to the mass of the force carrier	13
5	Summary	14

1 Introduction

Single component and collisionless cold dark matter (CCDM), which is treated as the standard dark matter (DM) candidate in Λ CDM model, accounts for the cosmological data from Cosmic Microwave Background (CMB), Big Bang Nucleosynthesis (BBN), and the large scale structure. However, the above DM properties lead to some controversies between the N-body simulation and astrophysical observations on small scale structures with non-linear DM-dominated systems. A cusp structure is formed by gravitationally attracting a large number of DM in the center regions of galaxies and the zero dissipative dynamics [1]. On the other hand, observations indicate that DM distributes in a much more flat profile in the center regions [2, 3]. This is called the cusp/core problem [4]. There exists other problem with CCDM concerning the size of subhalos, which are the hosts of the satellite galaxies surrounding the Milky Way (MW) halo. The dispersion velocities from these galaxy rotation curves reflect the size of their host subhalos. It is observed that a discrepancy in the subhalo size exists between the CCDM-only simulation and the observations [5–7]. About $\mathcal{O}(10)$ most massive subhalos generated from the N-body simulation are too massive in the MW halo (with circular velocity larger than 30 km/s) whereas the maximum circular velocities of MW dwarf spheroidals are less than 25 km/s. This is referred to as the “Too-big-to-fail” problem indicating no satellite galaxy hosted by such massive subhalo is found.

It is possible that these puzzles may be due to insufficient knowledge of the baryonic processes such as the supernova feedback and photonization [8–14]. On the other hand, these conflicts may also hint nontrivial features of DM such as self-interacting DM (SIDM) [15]. It was then noted that the SIDM with a constant cross section cannot account for observed ellipticities in clusters [16, 17] and the survivability of subhalos [18]. In the very short mean free path limit, it produces even more cuspy profiles [19–22]. However, some recent simulations have shown that the SIDM velocity-independent cross sections in the range $\sigma_T/m_\chi \sim 0.1$ – 10 cm²/g (m_χ denoting the DM mass) can resolve the cusp/core and Too-big-to-fail problems on dwarf scales [23–26], although it was pointed out in ref. [24] that $\sigma_T/m_\chi \sim 0.1$ cm²/g

is too small to account for the population of massive subhalos, and the study using bullet cluster 1E 0657-56 constrains σ_T/m_χ to be less than $1.25 \text{ cm}^2/\text{g}$ [27]. Furthermore, other investigations of SIDM with characteristic velocity-dependent cross sections provide a broader cross section range, $\sigma_T/m_\chi \sim 0.1\text{--}50 \text{ cm}^2/\text{g}$, for alleviating the above-mentioned puzzles [28–33].¹ From particle physics point of view, DM exchanging light mediators would generate an attractive self-interaction, which enhances the annihilation cross section by Sommerfeld effect and resonance scattering [36, 37]. The mediator ϕ often plays as the messenger between the visible matter and dark matter. This mediator can be scalar, pseudoscalar, vector, or axial-vector particles [38]. The DM-nucleon interaction through scalar or vector mediator leads to spin-independent (SI) cross section (in the non-relativistic limit), while spin-dependent cross section results from exchanging pseudoscalar or axial-vector particle. The relatively large SIDM cross section requires a MeV scale ϕ satisfying [31, 32]

$$\sigma_{\chi\chi} \approx 7.6 \times 10^{-24} \text{ cm}^2 \left(\frac{\alpha_\chi}{0.01}\right)^2 \left(\frac{m_\phi}{30 \text{ MeV}}\right)^{-4} \left(\frac{m_\chi}{\text{GeV}}\right)^2, \quad (1.1)$$

where α_χ is the dark fine structure constant representing the coupling strength between DM χ and the mediator ϕ . With m_ϕ around the MeV scale, it is possible for ϕ to decay into light standard model particles. In such a case, the lifetime of ϕ should be less than 1 sec to satisfy the BBN constraint.² Therefore, the light mediator ϕ can produce both direct and indirect DM signatures. The former signature is generated when DM scatters with the nuclei by exchanging ϕ . The latter signature is generated by the annihilation of DMs into a pair of ϕ , which subsequently decay into SM particles. The mediator ϕ can be a hidden U(1) gauge boson or scalar, which mixes with photon, Z boson or Higgs boson to bridge between DM and the visible sectors. It should be noted that eq. (1.1) is valid only at the perturbative regime ($\alpha_\chi m_\chi/m_\phi \leq 1$), while the effects of dark force on the halo structure for the full range of parameters were investigated in refs. [31, 32]. The characteristic velocity-dependent cross section at different scales for resolving all the conflicts can be realized. Furthermore, DM direct detection experiments for probing such SIDM scenarios were proposed in ref. [40] (see also, for example, ref. [41] for the asymmetric DM scenario). The predicted direct detection cross section is within the reach of next-generation experiments such as XENON1T [42] and SuperCDMS [43].

In this paper, we shall consider symmetric fermionic DM and show that the annihilation signatures from the trapped DMs inside the Sun can provide a complementary test to SIDM scenarios. It is well known that the DM-nucleon scattering cross section relevant to the indirect DM signature from the Sun is identical to the cross section relevant to DM direct detection experiments. For the former case, such a cross section leads to the DM capture if the velocity of the final-state DM is less than the escape velocity of the Sun. As the number of captured DMs increases to a significant level, the rate of DM annihilations into SM particles could become detectable [44–53]. The total number of the captured DMs is determined by the above DM-nucleon scattering cross section and the DM mass. However, it has been shown in a model-independent approach that the DM accumulation time can be shortened in the Sun and the total number of trapped DM can also be increased if SIDM is considered [51–53]. In ref. [52], the constraint $\sigma_T < \mathcal{O}(10^{-22}) \text{ cm}^2$ is obtained for the $\chi\chi \rightarrow W^+W^-/\tau^+\tau^-$

¹The thorough study on cosmology and structure formation in the context of mirror photon is investigated in ref. [34]. Some early attempts to study the astrophysical effects of mirror matters can also be found, for example, in ref. [35].

²If DM is kinematically decoupled from the dark radiation at late time, it would leave signals in CMB [39].

annihilation mode using IceCube 79 string data [54] which probes the mass range $m_\chi > 20$ GeV. The low-mass DM region to be probed by IceCube-PINGU is considered in ref. [53]. In this work we shall present a realization of the above model-independent results with a concrete SIDM model. We work out the SIDM model prediction on the DM-induced neutrino flux from the Sun and the sensitivities of future neutrino telescopes to such a signal and the related model parameters. We compare these sensitivities to constraints set by current direct detection experiments. We will show that the searches for direct and indirect DM signals give complementary tests to the parameter space of SIDM model. The complementarity of direct and indirect searches arises from two reasons. First, the indirect search can look for very light DM which is not yet probed by direct detections.³ Second, the direct detection sensitivity could be significantly worsen by isospin violation in DM-nucleon couplings. On the other hand, the DM-induced neutrino flux from the Sun can be insensitive to DM-nucleus scattering cross section so long as DM self-interaction is strong enough [51, 53].

Our paper is organized as follows. In section 2 we briefly introduce the SIDM models where the light mediator is either a gauge boson or a scalar particle. The constraints on these models are summarized. Section 3 shows that the DM accumulation inside the Sun can be significantly enhanced by DM self-interaction. In section 4, we demonstrate that IceCube/PINGU experiment can probe SIDM parameters in a way complementary to the direct detection experiment. We present our conclusions in section 5.

2 Scattering via light mediator exchange

Two generic ways to construct the SIDM model are to assume a light vector boson or a light scalar boson as the dark force mediator.⁴ For the vector mediator case, DM carries a charge e_D under a hidden Abelian $U(1)_\chi$ gauge symmetry and ϕ^μ is the corresponding gauge boson. The hidden $U(1)_\chi$ gauge boson has no ordinary SM interaction except the one induced by kinetic mixing with the SM photon [58]. Since we expect the mass of dark mediator ϕ to be around MeV scale, there must exist certain mechanism to generate a massive $U(1)_\chi$ gauge boson. It can be certain spontaneous symmetry breaking pattern in the dark sector or based upon the Stueckelberg mechanism [59, 60] to ensure the UV completion of the theory. Here we take the phenomenological approach and neglect the details of model construction. The $\phi\gamma$ and ϕZ mixings lead to the following couplings between ϕ^μ and SM currents:

$$\mathcal{L}_{\text{mixing/vector}} = \left(\epsilon_\gamma e J_{\text{em}}^\mu + \epsilon_Z \frac{g_2}{c_W} J_{\text{NC}}^\mu \right) \phi_\mu, \quad (2.1)$$

with

$$J_{\text{em}}^\mu = \sum_f Q_f \bar{f} \gamma^\mu f \quad \text{and} \quad J_{\text{NC}}^\mu = \sum_f \bar{f} \gamma^\mu \left[I_{3f} \left(\frac{1 - \gamma_5}{2} \right) - Q_f s_W^2 \right] f \quad (2.2)$$

representing electromagnetic current and weak neutral current respectively. Here f is the SM fermion and Q_f refers to its electric charge, g_2 is the $SU(2)_L$ gauge coupling, and $c_W(s_W) =$

³We should mention that there exist a few ongoing direct search experiments aiming to detect the low mass WIMP. The DAMIC experiment set upper limits on the spin-independent cross section (10^{-38} – 10^{-39} cm²) for WIMPs below 4 GeV [55]. The CRESST-II collaboration puts a slightly stronger bound for WIMPs below 3 GeV and its sensitivity can be extended to the sub-GeV region [56]. The range of the WIMP-nucleon SI cross sections between 10^{-38} – 10^{-41} cm² is excluded for WIMP mass between 1.6 GeV and 5.5 GeV by the second CDMSlite run [57].

⁴In this paper, we analyze the case of velocity-independent cross sections.

$\cos\theta_W(\sin\theta_W)$. The parameters ε_γ and ε_Z are originated from kinetic and mass mixings between ϕ^μ and gauge bosons such as

$$\mathcal{L}_{\text{mixing, U(1)}} = \frac{\varepsilon_\gamma}{2}\phi_{\mu\nu}F^{\mu\nu} + \varepsilon_Z m_Z^2 \phi_\mu Z^\mu. \quad (2.3)$$

With DM χ a Dirac fermion, the dark force is given by

$$\mathcal{L}_{\text{DM}_{\phi_{\text{vector}}}} = e_D \bar{\chi} \gamma^\mu \chi \phi_\mu. \quad (2.4)$$

For the case of scalar ϕ , it is possible that ϕ can mix with Higgs boson. The simplest scenario is that ϕ is a real singlet scalar. The relevant terms of the Lagrangian are then given by

$$\mathcal{L}_{\text{DM}_{\phi_{\text{scalar}}}} \supset g_s \bar{\chi} \chi \phi + a\phi |H|^2 + b\phi^2 |H|^2, \quad (2.5)$$

where g_s , a , and b are coupling constants and H is the SM Higgs doublet. As the Higgs boson develops the vacuum expectation value $v \approx 246$ GeV, the mass matrix between ϕ and H can mix via the a term. We can define the mixing parameter $\varepsilon_h \sim av/m_h^2$, thus the effective Lagrangian for the coupling of scalar ϕ to the SM fermions is given by

$$\mathcal{L}_{\text{mixing/scalar}} = \sum_f -\varepsilon_h \frac{m_f}{v} \bar{f} f. \quad (2.6)$$

2.1 Scattering with vector mediator

The Feynman diagrams for scattering among two Dirac fermionic (anti-) DMs via the dark mediator ϕ are depicted in figure 1. Due to Fermi statistics, the u and t channel amplitudes of $\chi\chi$ scattering carry a relative minus sign such that two amplitudes cancel each other in the non-relativistic limit. The same cancellation occurs in $\bar{\chi}\bar{\chi}$ scattering. Hence only $\chi\bar{\chi}$ scattering cross section is nonvanishing in the non-relativistic limit. Furthermore, the s channel amplitude of $\chi\bar{\chi}$ scattering is suppressed so long as $m_\chi \gg m_\phi$. Hence we consider only t channel amplitude for $\chi\bar{\chi}$ scattering. The perturbative calculation gives the cross section

$$\sigma_{\chi\bar{\chi}} \approx 4\pi\alpha_\chi^2 \frac{m_\chi^2}{m_\phi^4}, \quad (2.7)$$

where $\alpha_\chi \equiv e_D^2/(4\pi)$ is the fine structure constant in the hidden U(1) sector. Since only $\sigma_{\chi\bar{\chi}}$ is not suppressed for Dirac DM, the parameterization in eq. (1.1) should be understood as the one for $\sigma_{\chi\bar{\chi}}$. In fact, for simplifying the notations, we henceforth denote the $\chi\bar{\chi}$ scattering cross section as $\sigma_{\chi\chi}$.

The DM-nucleon scattering is shown in figure 2 where N stands for either proton or neutron. The parameter ε_N is the strength of ϕ_μ -nucleon coupling in the unit of electric charge e . The SI cross section between DM and any nucleus with mass number A and proton number Z is then given by

$$\sigma_{\chi A} \approx \frac{16\pi\alpha_\chi\alpha_{\text{em}}}{m_\phi^4} [\varepsilon_p Z + \varepsilon_n(A-Z)]^2 \mu_{\chi A}^2 = \frac{16\pi\alpha_\chi\alpha_{\text{em}}}{m_\phi^4} \varepsilon_p^2 [Z + \eta(A-Z)]^2 \mu_{\chi A}^2, \quad (2.8)$$

with α_{em} the fine structure constant, $\mu_{\chi A} \equiv m_\chi m_A/(m_\chi + m_A)$ the reduced mass for DM-nucleus system and $\eta \equiv \varepsilon_n/\varepsilon_p$ the isospin violation parameter. The cross section for $\bar{\chi}$

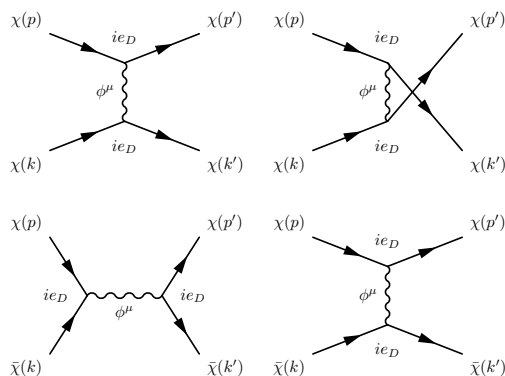


Figure 1. The Feynman diagrams contributing to DM scatterings. The upper panel represents the t and u channel diagrams of $\chi\chi$ scattering. The lower one represents the s and t channel diagrams of $\chi\bar{\chi}$ scattering. The $\chi\chi$ cross section vanishes in the non-relativistic limit while $\chi\bar{\chi}$ scattering is dominated by the t channel diagram. The behavior of $\bar{\chi}\bar{\chi}$ scattering is the same as that of $\chi\chi$ scattering. See the main text for details.

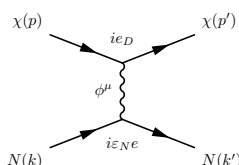


Figure 2. The Feynman diagram contributing to χ - N scattering. One simply replaces χ by $\bar{\chi}$ in the diagram for $\bar{\chi}$ - N scattering.

is identical such that $\sigma_{\chi A} = \sigma_{\bar{\chi} A}$. The effective ϕ_μ -nucleon couplings, ε_p and ε_n , can be expressed in terms of ε_γ and ε_Z such that [40]

$$\varepsilon_p = \varepsilon_\gamma + \frac{\varepsilon_Z}{4s_W c_W} (1 - 4s_W^2) \approx \varepsilon_\gamma + 0.05\varepsilon_Z, \quad (2.9a)$$

$$\varepsilon_n = -\frac{\varepsilon_Z}{4s_W c_W} \approx -0.6\varepsilon_Z. \quad (2.9b)$$

Thus, we have SI cross sections

$$\sigma_{\chi p}^{\text{SI}} \approx 1.5 \times 10^{-24} \text{ cm}^2 \varepsilon_\gamma^2 \left(\frac{\alpha_\chi}{0.01} \right) \left(\frac{m_\phi}{30 \text{ MeV}} \right)^{-4} \quad (2.10)$$

for DM-proton scattering and

$$\sigma_{\chi n}^{\text{SI}} \approx 5 \times 10^{-25} \text{ cm}^2 \varepsilon_Z^2 \left(\frac{\alpha_\chi}{0.01} \right) \left(\frac{m_\phi}{30 \text{ MeV}} \right)^{-4} \quad (2.11)$$

for DM-neutron scattering.

2.2 Scattering with scalar mediator

The Feynman diagrams for DM-DM scattering with scalar exchange are identical to those depicted in figure 1. Thus we only replace α_χ by $\alpha_s = g_s^2/4\pi$, and the mixing parameter ε_h via the Higgs boson are the same for both proton and neutron. Roughly one has

$$\varepsilon_{p,n} \approx 3 \times 10^{-3} \varepsilon_h. \quad (2.12)$$

The general DM-nucleon cross section thus obeys the isospin symmetry with

$$\sigma_{\chi N} \approx 2 \times 10^{-29} \text{ cm}^2 \varepsilon_h^2 \left(\frac{\alpha_s}{0.01} \right) \left(\frac{m_\phi}{30 \text{ MeV}} \right)^{-4}. \quad (2.13)$$

However, to have ϕ decay before BBN, one requires $\varepsilon_h \gtrsim 10^{-5}$. With such a lower bound for ε_h , the resulting $\sigma_{\chi p}$ is so large that it is excluded by the current direct search for $m_\chi > 10 \text{ GeV}$ [40]. In this work, we shall not continue discussing the scalar case, although some other scalar-exchange models might still be viable. It is important to note that the vector mediator case already contains many features of SIDM models. In addition, we are interested in searching for neutrino signals. Such type of signals disfavors the scalar mediator since the decay branching ratios of ϕ to neutrinos are generally negligible, unless $m_\phi < 1 \text{ MeV}$. We note that the spin-dependent DM-nucleon cross section is suppressed by $\mathcal{O}(1/m_\chi)$ for the case of vector mediator. On the other hand, such suppression does not occur if ϕ is an axial-vector particle. In this paper, we shall only focus on spin-independent cross section. Hence we simplify $\sigma_{\chi p}^{\text{SI}}$ as $\sigma_{\chi p}$ from now on.

3 DM accumulation in the Sun

3.1 The evolution equation

Since we consider the scenario that χ and $\bar{\chi}$ are equally populated, the halo DM number density near the solar system can then be written as $\rho_0 = \rho_\chi + \rho_{\bar{\chi}} = 0.3 \text{ GeV cm}^{-3}$ with $\rho_\chi = \rho_{\bar{\chi}} = 0.15 \text{ GeV cm}^{-3}$. The DM in the Sun consists of two species, the DM and anti-DM with the numbers N_χ and $N_{\bar{\chi}}$ respectively. The time evolutions of N_χ and $N_{\bar{\chi}}$ are given by

$$\frac{dN_\chi}{dt} = C_c - C_e N_\chi + C_s N_{\bar{\chi}} - (C_a + C_{se}) N_\chi N_{\bar{\chi}}, \quad (3.1a)$$

$$\frac{dN_{\bar{\chi}}}{dt} = C_c - C_e N_{\bar{\chi}} + C_s N_\chi - (C_a + C_{se}) N_{\bar{\chi}} N_\chi, \quad (3.1b)$$

with C_c the capture rate, C_e the evaporation rate, C_s the capture rate due to self-interaction, C_{se} the self-interaction induced evaporation rate, and C_a the annihilation rate. They are taken to be time-independent and have been fully discussed in refs. [46–51, 53] and references therein.

The capture rates C_c and C_s depend on DM-nucleus scattering cross section $\sigma_{\chi A}$ and DM-DM self-interaction cross section $\sigma_{\chi\chi}$, respectively. For a MeV range m_ϕ , it has been pointed out that [40, 61] $\sigma_{\chi A}$ is sensitive to the momentum transfer \mathbf{q} flowing into the ϕ propagator shown in figure 2. We thus have

$$\sigma_{\chi A}(\mathbf{q}^2) = \frac{m_\phi^4}{(m_\phi^2 + \mathbf{q}^2)^2} \sigma_{\chi A}^0 \quad (3.2)$$

where the magnitude of momentum transfer is given by $\mathbf{q}^2 = 2m_A E_R$ with E_R the nucleus recoil energy, and $\sigma_{\chi A}^0 \equiv \sigma_{\chi A}(\mathbf{q}^2 = 0)$ is the cross section with zero momentum transfer. It is clearly seen that $\sigma_{\chi A}(\mathbf{q}^2)$ is suppressed compared to $\sigma_{\chi A}^0$. For estimating this suppression, we take $E_R = 2\mu_{\chi A}^2 v_\chi^2 / m_A$ with $\mu_{\chi A}$ the reduced mass for the DM-nucleus system. This E_R corresponds to an 180° DM recoil angle after the collision in the center of momentum frame. We further take $v_\chi \approx 270 \text{ km/s}$, which is the DM velocity dispersion in the halo.

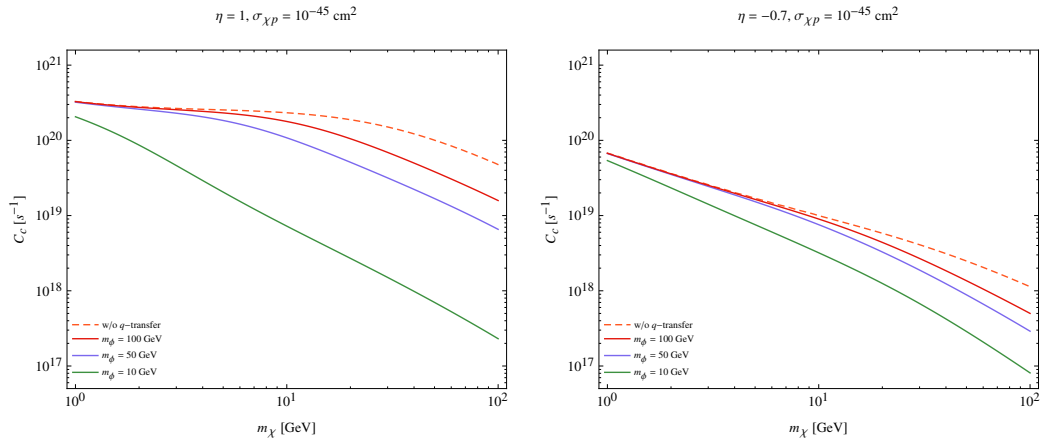


Figure 3. The capture rates with (solids) and without momentum transfer (dashed). The cross section $\sigma_{\chi p}^0 = 10^{-45} \text{ cm}^2$ for all results. Left and right are corresponding to $\eta = 1$ and -0.7 .

Apparently, \mathbf{q}^2 depends on both m_A and m_χ . Thus, the capture rate with the momentum transfer suppression can be expressed as

$$C_c \propto \left(\frac{\rho_\chi}{0.15 \text{ GeV/cm}^3} \right) \left(\frac{\text{GeV}}{m_\chi} \right) \left(\frac{270 \text{ km/s}}{v_\chi} \right) \sum_A F_A(m_\chi, \eta) \sigma_{\chi A}^0 \frac{m_\phi^4}{(m_\phi^2 + \mathbf{q}^2)^2}, \quad (3.3)$$

where $F_A(m_\chi, \eta)$ is the product of various factors relevant to the chemical element A in the Sun, including the mass fraction, chemical element distribution, kinematic suppression, form factor, reduced mass and isospin violation effect. In figure 3, we compare the effect of momentum transfer suppression on C_c for different m_ϕ with $\sigma_{\chi p}^0$ fixed at 10^{-45} cm^2 . One can see that the momentum transfer suppression is more severe for larger m_χ since \mathbf{q}^2 increases with m_χ .

The above momentum transfer suppression also occurs in C_s . The suppression factor can be taken from eqs. (3.2) and (3.3). Thus

$$C_s(\mathbf{q}^2) \propto \left(\frac{\rho_\chi}{0.15 \text{ GeV/cm}^3} \right) \left(\frac{\text{GeV}}{m_\chi} \right) \left(\frac{270 \text{ km/s}}{v_\chi} \right) \sigma_{\chi\chi}^0 \langle \hat{\phi} \rangle \frac{\text{erf}(\eta)}{\eta} \frac{m_\phi^4}{(m_\phi^2 + \mathbf{q}^2)^2} \quad (3.4)$$

with $\sigma_{\chi\chi}^0$ the cross section of DM-DM scattering at $\mathbf{q}^2 = 0$, $\langle \hat{\phi} \rangle = 5.1$ the average gravitational potential in the core, $\eta = 3(v_\odot/v_\chi)^2/2 \approx 1.1$ a dimensionless constant and $v_\odot = 220 \text{ km s}^{-1}$ the relative velocity of the Sun to the Galactic center. For DM self-capture, we have $\mathbf{q} = m_\chi(\mathbf{v}_i - \mathbf{v}_f)$ where \mathbf{v}_i is the DM velocity before the scattering with the magnitude of the velocity given by $v_i = \sqrt{v_\chi^2 + v_{\text{esc}}(r)^2}$, while \mathbf{v}_f is the DM velocity after the scattering with $v_f = v_{\text{esc}}(r)/\sqrt{2}$ on average [62]. We take the approximation that \mathbf{v}_f is parallel to \mathbf{v}_i since the speed of halo DM is in general much greater than that of the trapped DM.

Having discussed the properties of C_c and C_s , we return to eqs. (3.1a) and (3.1b). Since we are interested in the symmetric DM, the condition $N_\chi = N_{\bar{\chi}}$ holds. Thus, eqs. (3.1a) and (3.1b) can be simplified into one,

$$\frac{dN_\chi}{dt} = C_c - C_e N_\chi + C_s N_\chi - (C_a + C_{se}) N_\chi^2, \quad (3.5)$$

with the solution

$$N_\chi(t) = \frac{C_c \tanh(t/\tau_A)}{\tau_A^{-1} - (C_s - C_e) \tanh(t/\tau_A)/2}, \quad (3.6)$$

where

$$\tau_A \equiv \frac{1}{\sqrt{C_c(C_a + C_{se}) + (C_s - C_e)^2/4}} \quad (3.7)$$

is the time-scale for the DM number in the Sun to reach the equilibrium, i.e., $dN_\chi/dt = 0$. The DM number reaches the equilibrium when $\tanh(t/\tau_A) \sim 1$.

The DM annihilation rate in the Sun is given by

$$\Gamma_A = C_a N_\chi N_{\bar{\chi}} = C_a N_\chi^2, \quad (3.8)$$

where the annihilation cross section $\langle\sigma v\rangle$ appearing in C_a is taken to be $6 \times 10^{-26} \text{ cm}^3 \text{ s}^{-1}$ for Dirac fermion DM. By setting $C_s = C_{se} = 0$, we recover the results in refs. [46–50] for the absence of DM self-interaction. By setting $C_e = C_{se} = 0$, we recover the result in ref. [51], which includes the DM self-interaction while neglects the DM evaporation.

3.2 Numerical results

To illustrate the role of the light force carrier m_ϕ , we first identify the parameter range on the m_χ - m_ϕ plane in which $N_\chi(t)$ has already reached to the equilibrium at the present epoch. In the hidden U(1) model, isospin violation is generally introduced since η can take any value [63]. However, to simplify our discussions, we consider two extreme scenarios in our calculation. One is the isospin symmetric scenario with $\eta = 1$, and the other corresponds to $\eta = -0.7$ which minimizes DM-Xenon cross section for a fixed $\sigma_{\chi p}$ [64]. The first scenario corresponds to $\varepsilon_\gamma/\varepsilon_Z = -0.65$ while the second one corresponds to $\varepsilon_\gamma/\varepsilon_Z = 5.65$.

In figure 4, we show the equilibrium regions for $\varepsilon_\gamma = 10^{-9}$ and 10^{-10} [65, 66] with $\eta = 1$ and $\eta = -0.7$, respectively. The dense color regions circled by the thick lines are the parameter ranges where the equilibrium has not yet reached in the current epoch. We quantify such regions by $\tanh(t/\tau_A) < 0.99$. To the left of the gray dashed line, DMs in the Sun evaporate and consequently unable to produce detectable signals. In contrast, the equilibrium is between the capture and the annihilation to the right of the gray dashed line. In this region, the captured DM number is at the maximum, hence the annihilation rate is at its maximum as well. It is of interest to compare the size of non-equilibrium region for different combinations of ε_γ and η in figure 4. One can see from eq. (3.7) that a smaller C_c leads to a larger equilibrium time scale τ_A provided all the other coefficients are held fixed. Comparing the left and right panels of figure 4, it is seen that the non-equilibrium region increases tremendously as ε_γ lowering from 10^{-9} to 10^{-10} . In fact, one can see from eq. (2.10) that $\sigma_{\chi p}$ decreases by two orders of magnitude when ε_γ decreases by an order of magnitude. Hence the DM-nucleus cross section $\sigma_{\chi A}$ and consequently the C_c are also significantly reduced. This leads to a larger equilibrium time scale as just argued. For $\varepsilon_\gamma = 10^{-9}$, the non-equilibrium region also increases with η lowering from 1 to -0.7 . This is also due to the suppression of $\sigma_{\chi A}$ caused by isospin violation. However, with $\varepsilon_\gamma = 10^{-10}$, the non-equilibrium region does not change noticeably when η changes from 1 to -0.7 . One can see that for such an ε_γ the equilibrium is reached at $m_\phi \sim \mathcal{O}(1) \text{ MeV}$ and m_χ of a few GeVs. This indicates that DM self-interaction is significant in this parameter region.

The theoretical predictions on $\sigma_{\chi p}$ are shown in figure 5 with colored solid lines. These predictions are according to eq. (2.10) and the additional momentum transfer suppression

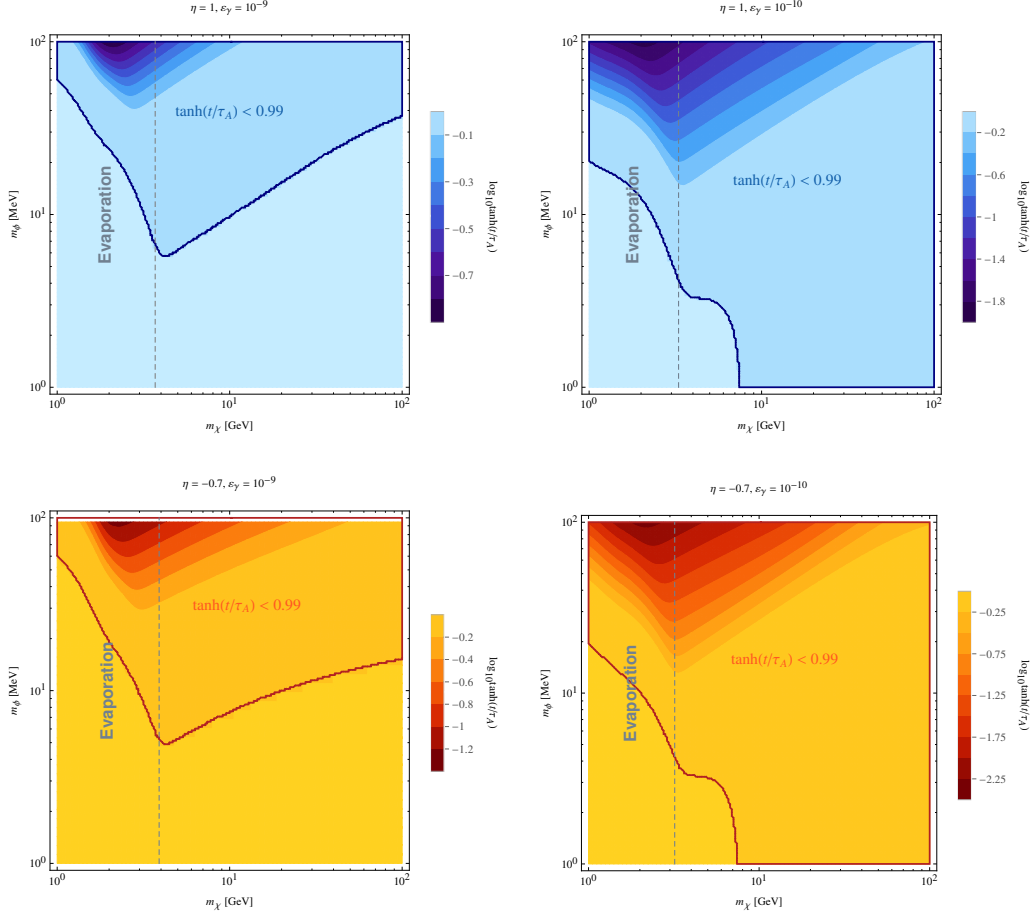


Figure 4. The dependencies of $\tanh(t_{\odot}/\tau_A)$ on m_{χ} and m_{ϕ} for $\varepsilon_{\gamma} = 10^{-9}$ (left) and 10^{-10} (right). The regions circled by thick lines are the parameter ranges in which the DM number $N_{\chi, \bar{\chi}}$ have not yet reached the equilibrium in the current epoch. The region to the left of the dash line is the parameter space that DM evaporation takes place. This is the non-detection region for the indirect DM search. The upper panel is for the isospin symmetric case while the lower one is for the isospin violation case.

given by eq. (3.2). It is seen that $\sigma_{\chi p}$ depends on ε_{γ} , α_{χ} and m_{ϕ} . However, α_{χ} is related to m_{χ} by $\alpha_{\chi} \approx 3.3 \times 10^{-5} (m_{\chi}/\text{GeV})$ from the thermal relic density of symmetric DM [40, 67]. The regions excluded by LUX [68] for the scenarios of isospin symmetry and isospin violation are displayed for comparisons. The orange band is the allowed region of the SIDM parameter space $\sigma_T/m_{\chi} \sim 0.1\text{--}10 \text{ cm}^2/\text{g}$ [23–26].

The value of η affects the DM-nucleus cross section as seen from eq. (2.8). Hence $\eta \neq 1$ (isospin violation) may weaken the direct search bound on $\sigma_{\chi p}$ as well as suppress the capture rate for both the Sun and the Earth for a fixed $\sigma_{\chi p}$ as discussed in refs. [69–71]. It is clearly seen that the LUX bound on $\sigma_{\chi p}$ is significantly weakened for $\eta = -0.7$.

The evolution behaviors of N_{χ} with different m_{χ} , m_{ϕ} and η are shown in figure 6. The difference in N_{χ} between $\eta = 1$ and $\eta = -0.7$ is easy to understand. It is clear that C_c with $\eta = -0.7$ is suppressed compared to C_c with $\eta = 1$. Hence N_{χ} with $\eta = 1$ is greater than N_{χ} with $\eta = -0.7$ no matter how large C_s is. Moreover, comparing the upper right panel with the upper left one in figure 6, we find that N_{χ} is less affected by η in the former case for the same m_{χ} . The DM-nucleus cross section $\sigma_{\chi A}$ for the upper right panel is suppressed due to

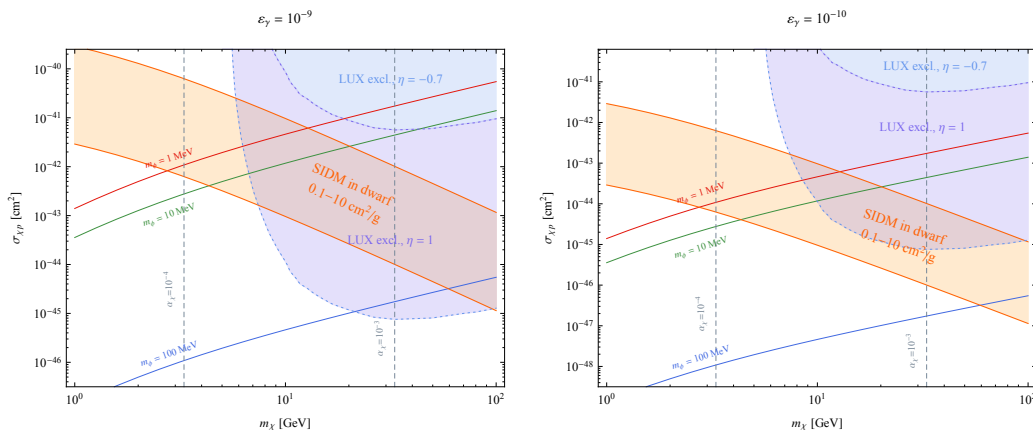


Figure 5. The theoretical predictions of $\sigma_{\chi\phi}$ with $m_\phi = 1$ MeV (red), 10 MeV (green) and 100 MeV (blue) are given in solid lines with $\varepsilon_\gamma = 10^{-9}$ (left panel) and 10^{-10} (right panel). The light and deep purple regions are excluded by LUX [68] for isospin symmetric and isospin violating scenarios, respectively. The orange band is the SIDM allowed region from the dwarf analysis [23–26]. See the main text for details.

a smaller ε_γ . Hence the effect from η becomes less significant. For lower left and lower right panels, we take $m_\phi = 100$ MeV. In this case, both $\sigma_{\chi A}$ and $\sigma_{\chi\chi}$ are suppressed. Hence the number of captured DM is much less and the equilibrium time scale is much larger compared to the corresponding quantities in the upper panels.

We have so far focused on the effect of C_c on N_χ . To quantify the effect by C_s , we present the ratio $N_\chi^{\text{self}}/N_\chi^0$ in figure 7 for $\eta = 1$ and -0.7 , where N_χ^{self} and N_χ^0 are the DM numbers with and without the contribution from C_s , respectively. With the contribution from C_s , N_χ can be almost twice larger than that without C_s . The enhancement by C_s is more significant for $\eta = -0.7$. Furthermore, such an enhancement is shifted to the larger m_χ when m_ϕ increases.

4 Testing SIDM model in IceCube-PINGU

4.1 Neutrino signal and the atmospheric background

Neutrino signals arise from the decays of ϕ which is produced by DM annihilation, i.e., $\chi\bar{\chi} \rightarrow \phi\phi \rightarrow 4\nu$. DM annihilate to ZZ and $\gamma\gamma$ modes are suppressed by small couplings between $\chi-Z$ and $\chi-\gamma$ respectively. For the hidden U(1) gauge model considered in this paper, ϕ decays into SM particles via ε_γ and ε_Z mixings. Due to the kinematics constraint, e^+e^- and neutrinos are the only decay products of ϕ and the corresponding decay widths through photon and Z mixings are given in ref. [40]. The branching ratio for $\phi \rightarrow \nu\bar{\nu}$ is determined by the relative magnitudes of mixing parameters ε_γ and ε_Z . Therefore it is determined by the parameter η through eqs. (2.9a) and (2.9a). We find $\text{BR}(\phi \rightarrow \nu\bar{\nu}) \approx 75\%$, 39% , 48% , and 67% for $\eta = 1, -0.3, -0.5$, and -0.7 , respectively. Furthermore, although ϕ is produced on-shell in the solar center, it does not decay instantly but instead propagates for a certain distance. The lifetime of ϕ is constrained by BBN, $\tau_\phi \lesssim \mathcal{O}(1)$ s [40, 66]. Considering a 30 MeV ϕ with 5 GeV energy (corresponding to $m_\chi = 10$ GeV), the decay time of ϕ would be less than 170 s. One can easily estimated that, for a ϕ with 170 s of decay time, it travels for roughly 5×10^7 km before decaying into the electron-positron or the neutrino pair. The

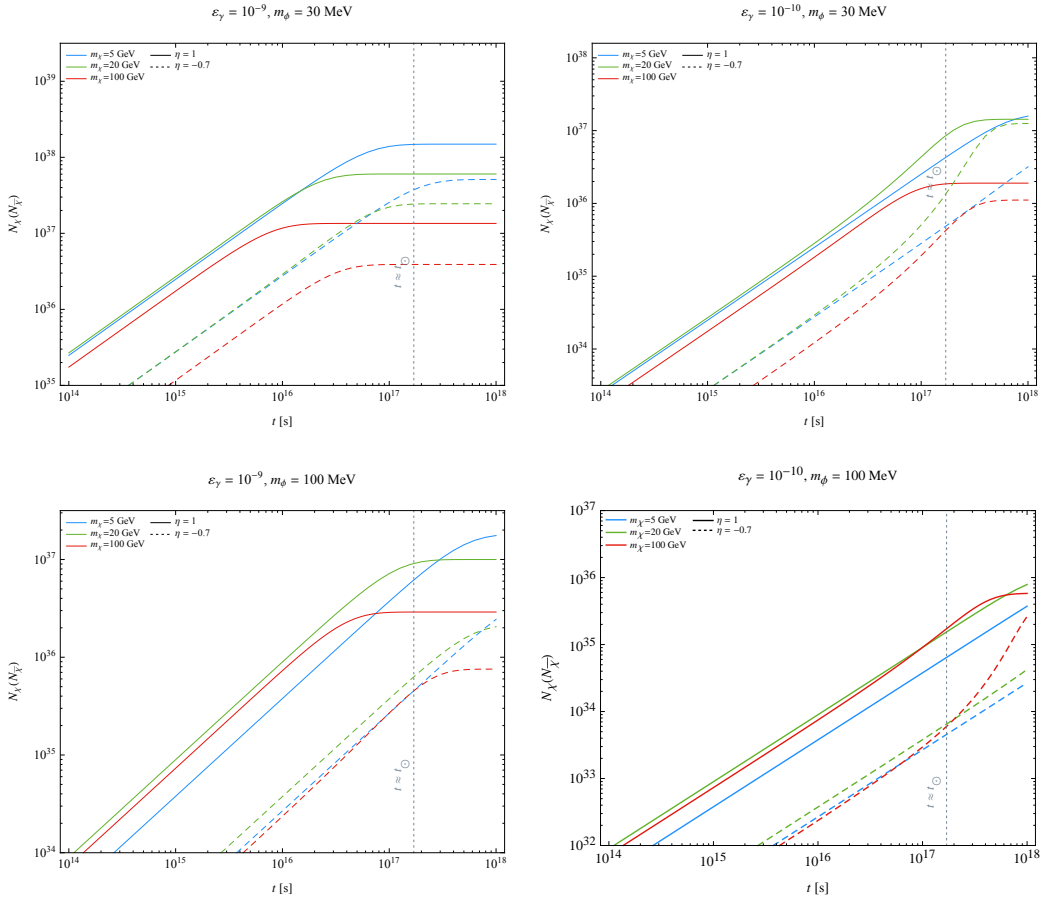


Figure 6. The $N_\chi(N_{\bar{\chi}})$ for $\varepsilon_\gamma = 10^{-9}$ (left column) and 10^{-10} (right column). The upper panels are for $m_\phi = 30$ MeV and the lower panels are for $m_\phi = 100$ MeV. Solid lines are for isospin symmetric case and dashed lines are for isospin violated case. Blue, green and red curves are for $m_\chi = 5$ GeV, 20 GeV and 100 GeV, respectively. The solar age (t_\odot) is indicated by the gray dashed line.

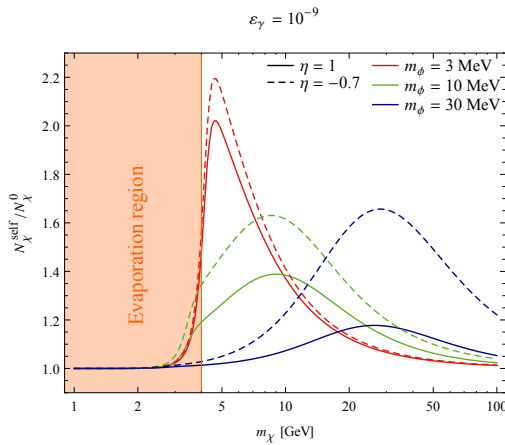


Figure 7. The ratio $N_\chi^{\text{self}}/N_\chi^0$ as a function of m_χ for $\varepsilon_\gamma = 10^{-9}$. Here N_χ^{self} and N_χ^0 are DM numbers with and without the contribution from C_s , respectively. See main text for details.

decay point is already outside the Sun but not yet reaching to the Earth. Given the distance between the Sun and the Earth at 1.5×10^8 km, those ϕ with 30 MeV of mass and moving toward the Earth shall decay between Sun and Earth provided E_ϕ is less than 150 GeV. Hence the neutrino flux will be observed by the terrestrial detector. We have so far made our argument with $\tau_\phi = 1$ s. For $\tau_\phi \ll 1$ s, the decay point of ϕ could be inside the Sun. In this case, the neutrino propagating distance from source to terrestrial detector becomes larger. However this does not affect the oscillation of neutrinos because neutrino propagating distances in both cases are much larger than the neutrino oscillation length. Hence our results on neutrino event rates are not affected.

The argument in the last paragraph assumes ϕ propagating freely inside the Sun. To justify this assumption, we study the interaction between ϕ and hydrogen, which occurs through the mixing between ϕ and γ and the subsequent γp scattering. The total γp scattering cross section at $\sqrt{s} = \sqrt{10}$ GeV is about 0.1 mb [73]. Taking $\varepsilon_\gamma = 10^{-9}$, we have ϕp total cross section as small as 10^{-46} cm². With the average hydrogen number density in the Sun about 6×10^{23} /cm³, the mean free path of ϕ is much greater than the radius of the Sun. We note that the consideration of other chemical elements in the Sun should shorten the mean free path of ϕ slightly. Nonetheless, this distance scale remains much greater than the radius of the Sun.

Since each ϕ stays at the same direction before its decay, one can view those neutrinos produced by ϕ decays as being originated from the core of the Sun. Hence we can write the neutrino flux as

$$\frac{d\Phi_{\nu_i}}{dE_{\nu_i}} = P_{\nu_j \rightarrow \nu_i}(E_\nu) \frac{\Gamma_A}{4\pi R^2} \frac{dN_{\nu_j}}{dE_{\nu_j}}, \quad (4.1)$$

with $P_{\nu_j \rightarrow \nu_i}(E_\nu)$ the neutrino oscillation during the propagation, Γ_A the DM annihilation rate, R the distance between Sun and Earth, and dN_{ν_j}/dE_{ν_j} the neutrino spectrum from each annihilation. The energy distribution dN_{ν_j}/dE_{ν_j} for neutrinos produced by ϕ decays is not a simple Dirac- δ function, since ϕ is highly boosted. It has been shown that [74]

$$\frac{dN_\nu}{dE_\nu} = \frac{4}{\Delta E} \Theta(E_\nu - E_-) \Theta(E_+ - E_\nu), \quad (4.2)$$

where Θ denotes the Heaviside step function. $E_\pm = (m_\chi \pm \sqrt{m_\chi^2 - m_\phi^2})/2$ are the maximum and minimum of the neutrino energy. $\Delta E \equiv \sqrt{m_\chi^2 - m_\phi^2}$ denotes the width of the energy spectrum.

The neutrino event rate in the detector is given by

$$N_\nu = \int_{E_{\text{th}}}^{m_\chi} \frac{d\Phi_{\nu_i}}{dE_{\nu_i}} A_\nu(E_\nu) dE_\nu d\Omega, \quad (4.3)$$

where E_{th} is the detector threshold energy, $A_\nu(E_\nu)$ the detector effective area and Ω the solid angle. We study both muon track events and cascade events induced by neutrinos. The DeepCore detector extends the IceCube capability to probe E_ν down to 10 GeV [76] and the future PINGU detector will further lower down the energy threshold E_{th} to $\mathcal{O}(1)$ GeV [77]. The angular resolution for IceCube-PINGU detector at $E_\nu = 5$ GeV is roughly 10° . Hence we consider neutrino events arriving from the solid angle range $\Delta\Omega = 2\pi(1 - \cos\psi)$ surrounding the Sun with $\psi = 10^\circ$. The detector effective area of IceCube is expressed as

$$A_\nu(E_\nu) = V_{\text{eff}} \frac{N_A}{M_{\text{ice}}} [n_p \sigma_{\nu p}(E_\nu) + n_n \sigma_{\nu n}(E_\nu)] \quad (4.4)$$

E_{\max} [GeV]	Track		Cascade	
	N_{ν}^{atm}	N_{ν}^{DM}	N_{ν}^{atm}	N_{ν}^{DM}
5	7146	76	9874	90
10	10280	91	13775	105
50	21680	132	21803	132
70	23584	138	23111	136
100	26610	146	24363	140

Table 1. The signal and background event numbers per year for reaching 2σ detection significance in 5 years.

with V_{eff} the energy-dependent detector effective volume [76, 77], N_A the Avogadro number, M_{ice} the molar mass of ice, $n_{p,n}$ the number density of proton/neutron per mole of ice, and $\sigma_{\nu p,n}$ the neutrino-proton/neutron cross section. One simply makes the replacement $\nu \rightarrow \bar{\nu}$ for anti-neutrino.

The atmospheric background is similar to eq. (4.3), by replacing $d\Phi_{\nu}/dE_{\nu}$ with atmospheric neutrino flux,

$$N_{\text{atm}} = \int_{E_{\text{th}}}^{E_{\max}} \frac{d\Phi_{\nu}^{\text{atm}}}{dE_{\nu}} A_{\nu}(E_{\nu}) dE_{\nu} d\Omega.$$

The $d\Phi_{\nu}^{\text{atm}}/dE_{\nu}$ is taken from ref. [78]. We set $E_{\max} = m_{\chi}$ in order to compare with DM signal.

4.2 The IceCube sensitivity to the mass of the force carrier

We present the sensitivity as a 2σ detection significance in 5 years, calculated with the formula,

$$\frac{s}{\sqrt{s+b}} = 2.0,$$

where s is the DM signal, b is the atmospheric background, and 2.0 is referring to the 2σ detection significance. The detector threshold energy E_{th} is set to be 1 GeV, which will be achieved by the future PINGU detector. Hence PINGU effective area is used for $1 \text{ GeV} \leq E_{\nu} \leq 10 \text{ GeV}$ while DeepCore effective area is applied for $E_{\nu} > 10 \text{ GeV}$. The annual signal and background event numbers for reaching 2σ detection significance in 5 years are listed in table 1. We present the track and cascade event numbers separately.

In figure 8, we present the IceCube-PINGU sensitivities to m_{ϕ} with different values of η in colored solid lines. Regions above these lines are beyond the reach of the detector within 5 years for a 2σ detection significance. Furthermore, each sensitivity curve terminates at the evaporation mass scale below which the DM signature from the Sun is suppressed. The left panel is for track events and the right one is for cascade events. BBN excludes $m_{\phi} < 20 \text{ MeV}$ for $\varepsilon_{\gamma} = 10^{-10}$, while it excludes $m_{\phi} < 0.3 \text{ MeV}$ for $\varepsilon_{\gamma} = 10^{-9}$. For simplicity, we only present results for $\varepsilon_{\gamma} = 10^{-9}$ since BBN constraint for $\varepsilon_{\gamma} = 10^{-10}$ rules out most of the m_{ϕ} parameter space shown here. The orange band is SIDM allowed region. Those color shaded regions are excluded by LUX for different η values. The gray dashed lines indicate the relation between α_{χ} and m_{χ} required by the thermal relic density.

It is of interest to compare results with different η values. It is seen that the sensitivity curve with $\eta = 1$ differs significantly from those with other η values. However, sensitivity

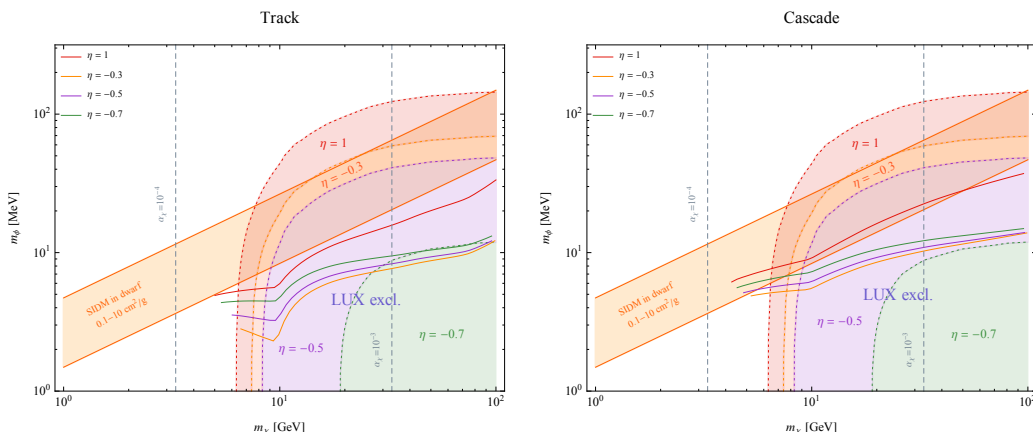


Figure 8. The 5-year IceCube-PINGU sensitivities (2σ) to m_ϕ for different values of η . The left panel is for track events and the right panel is for cascade events. The sensitivity curves and LUX excluded regions correspond to $\varepsilon_\gamma = 10^{-9}$. The results corresponding to $\varepsilon_\gamma = 10^{-10}$ are not shown since BBN constraint rules out most of the m_ϕ parameter space plotted here. The orange band is the SIDM allowed region described in figure 5.

curves with $-0.3 \leq \eta \leq -0.7$ do not differ much from one another. Clearly C_s rather than C_c dominates the DM capture in this range of η .

Comparing left and right panels of figure 8, one can see that cascade events can probe a larger part of $m_\chi - m_\phi$ parameter space. Furthermore, only cascade events can probe into the SIDM allowed region. Comparing IceCube-PINGU sensitivity with LUX constraint, the former complements the latter for low-mass DM until almost the evaporation mass scale $m_\chi \approx 4$ GeV. Such a complementarity also occurs due to isospin violation. It is well known that the direct search bound on $\sigma_{\chi p}$ could be significantly weakened by isospin violation. In fact, one can see that the LUX excluded region shrinks as η decreases from 1 to -0.7 . On the other hand, the indirect DM signature from the Sun is less affected by η . Hence the complementarity of two searches becomes more apparent when $\sigma_{\chi p}$ is subject to more severe isospin violation suppression.

5 Summary

We have proposed to test SIDM model with hidden U(1) gauge symmetry by searching for DM-induced neutrino signature from the Sun. The SIDM model under consideration gives rise to DM-nucleus scattering, DM-DM elastic scatterings, and DM-DM annihilation. These three processes determine the neutrino flux resulting from DM annihilation in the Sun. We have presented the IceCube-PINGU sensitivities to the parameter space of SIDM model. We compare these sensitivities to existing constraints set by LUX experiment. We have shown that the indirect search complements the direct one in two ways. First, the indirect search is more sensitive to light DM in GeV mass range. Second, the direct search constraint on SIDM parameter space can be significantly weakened by isospin violation while the indirect search sensitivity is less affected by this effect.

Acknowledgments

We thank R. Laha for pointing out ref. [74] to us. CSC is supported by the National Center for Theoretical Sciences, Taiwan; GLL and YHL are supported by Ministry of Science and Technology, Taiwan under Grant No. 103-2112-M-009-018.

References

- [1] J.F. Navarro, C.S. Frenk and S.D.M. White, *A Universal density profile from hierarchical clustering*, *Astrophys. J.* **490** (1997) 493 [[astro-ph/9611107](#)] [[INSPIRE](#)].
- [2] B. Moore, *Evidence against dissipationless dark matter from observations of galaxy haloes*, *Nature* **370** (1994) 629 [[INSPIRE](#)].
- [3] R.A. Flores and J.R. Primack, *Observational and theoretical constraints on singular dark matter halos*, *Astrophys. J.* **427** (1994) L1 [[astro-ph/9402004](#)] [[INSPIRE](#)].
- [4] M.G. Walker and J. Penarrubia, *A Method for Measuring (Slopes of) the Mass Profiles of Dwarf Spheroidal Galaxies*, *Astrophys. J.* **742** (2011) 20 [[arXiv:1108.2404](#)] [[INSPIRE](#)].
- [5] M.G. Walker, *Dark Matter in the Milky Way's Dwarf Spheroidal Satellites*, [arXiv:1205.0311](#) [[INSPIRE](#)].
- [6] M. Boylan-Kolchin, J.S. Bullock and M. Kaplinghat, *Too big to fail? The puzzling darkness of massive Milky Way subhaloes*, *Mon. Not. Roy. Astron. Soc.* **415** (2011) L40 [[arXiv:1103.0007](#)] [[INSPIRE](#)].
- [7] M. Boylan-Kolchin, J.S. Bullock and M. Kaplinghat, *The Milky Way's bright satellites as an apparent failure of Λ CDM*, *Mon. Not. Roy. Astron. Soc.* **422** (2012) 1203 [[arXiv:1111.2048](#)] [[INSPIRE](#)].
- [8] G. Efstathiou, *Suppressing the formation of dwarf galaxies via photoionization*, *Mon. Not. Roy. Astron. Soc.* **256** (1992) 43P [[INSPIRE](#)].
- [9] G. Efstathiou, J.R. Bond and S.D.M. White, *COBE Background radiation anisotropies and large scale structure in the universe*, *Mon. Not. Roy. Astron. Soc.* **258** (1992) 1 [[INSPIRE](#)].
- [10] M.-M. Mac Low and A. Ferrara, *Starburst-driven mass loss from dwarf galaxies: Efficiency and metal ejection*, *Astrophys. J.* **513** (1999) 142 [[astro-ph/9801237](#)] [[INSPIRE](#)].
- [11] J.S. Bullock, A.V. Kravtsov and D.H. Weinberg, *Reionization and the abundance of galactic satellites*, *Astrophys. J.* **539** (2000) 517 [[astro-ph/0002214](#)] [[INSPIRE](#)].
- [12] P.F. Hopkins, E. Quataert and N. Murray, *Stellar Feedback in Galaxies and the Origin of Galaxy-scale Winds*, *Mon. Not. Roy. Astron. Soc.* **421** (2012) 3522 [[arXiv:1110.4638](#)] [[INSPIRE](#)].
- [13] F. Governato et al., *Cuspy no more: how outflows affect the central dark matter and baryon distribution in Λ cold dark matter galaxies*, *Mon. Not. Roy. Astron. Soc.* **422** (2012) 1231 [[arXiv:1202.0554](#)] [[INSPIRE](#)].
- [14] A.M. Brooks and A. Zolotov, *Why Baryons Matter: The Kinematics of Dwarf Spheroidal Satellites*, *Astrophys. J.* **786** (2014) 87 [[arXiv:1207.2468](#)] [[INSPIRE](#)].
- [15] D.N. Spergel and P.J. Steinhardt, *Observational evidence for selfinteracting cold dark matter*, *Phys. Rev. Lett.* **84** (2000) 3760 [[astro-ph/9909386](#)] [[INSPIRE](#)].
- [16] N. Yoshida, V. Springel, S.D.M. White and G. Tormen, *Weakly self-interacting dark matter and the structure of dark halos*, *Astrophys. J.* **544** (2000) L87 [[astro-ph/0006134](#)] [[INSPIRE](#)].
- [17] J. Miralda-Escude, *A test of the collisional dark matter hypothesis from cluster lensing*, *Astrophys. J.* **564** (2002) 60 [[astro-ph/0002050](#)] [[INSPIRE](#)].
- [18] O.Y. Gnedin and J.P. Ostriker, *Limits on collisional dark matter from elliptical galaxies in clusters*, *Astrophys. J.* **561** (2001) 61 [[astro-ph/0010436](#)] [[INSPIRE](#)].
- [19] H.J. Mo and S. Mao, *Tully-fisher relation and its implications for halo density profile and self-interacting dark matter*, *Mon. Not. Roy. Astron. Soc.* **318** (2000) 163 [[astro-ph/0002451](#)] [[INSPIRE](#)].

- [20] C. Firmani, E. D’Onghia, V. Avila-Reese, G. Chincarini and X. Hernandez, *Evidence of self-interacting cold dark matter from galactic to galaxy cluster scales*, *Mon. Not. Roy. Astron. Soc.* **315** (2000) L29 [[astro-ph/0002376](#)] [[INSPIRE](#)].
- [21] B. Moore, S. Gelato, A. Jenkins, F.R. Pearce and V. Quilis, *Collisional versus collisionless dark matter*, *Astrophys. J.* **535** (2000) L21 [[astro-ph/0002308](#)] [[INSPIRE](#)].
- [22] N. Yoshida, V. Springel, S.D.M. White and G. Tormen, *Collisional dark matter and the structure of dark halos*, *Astrophys. J.* **535** (2000) L103 [[astro-ph/0002362](#)] [[INSPIRE](#)].
- [23] M. Vogelsberger, J. Zavala and A. Loeb, *Subhaloes in Self-Interacting Galactic Dark Matter Haloes*, *Mon. Not. Roy. Astron. Soc.* **423** (2012) 3740 [[arXiv:1201.5892](#)] [[INSPIRE](#)].
- [24] J. Zavala, M. Vogelsberger and M.G. Walker, *Constraining Self-Interacting Dark Matter with the Milky Way’s dwarf spheroidals*, *Mon. Not. Roy. Astron. Soc.* **431** (2013) L20 [[arXiv:1211.6426](#)] [[INSPIRE](#)].
- [25] M. Rocha et al., *Cosmological Simulations with Self-Interacting Dark Matter I: Constant Density Cores and Substructure*, *Mon. Not. Roy. Astron. Soc.* **430** (2013) 81 [[arXiv:1208.3025](#)] [[INSPIRE](#)].
- [26] A.H.G. Peter, M. Rocha, J.S. Bullock and M. Kaplinghat, *Cosmological Simulations with Self-Interacting Dark Matter II: Halo Shapes vs. Observations*, *Mon. Not. Roy. Astron. Soc.* **430** (2013) 105 [[arXiv:1208.3026](#)] [[INSPIRE](#)].
- [27] S.W. Randall, M. Markevitch, D. Clowe, A.H. Gonzalez and M. Bradac, *Constraints on the Self-Interaction Cross-Section of Dark Matter from Numerical Simulations of the Merging Galaxy Cluster 1E 0657-56*, *Astrophys. J.* **679** (2008) 1173 [[arXiv:0704.0261](#)] [[INSPIRE](#)].
- [28] J.L. Feng, M. Kaplinghat and H.-B. Yu, *Halo Shape and Relic Density Exclusions of Sommerfeld-Enhanced Dark Matter Explanations of Cosmic Ray Excesses*, *Phys. Rev. Lett.* **104** (2010) 151301 [[arXiv:0911.0422](#)] [[INSPIRE](#)].
- [29] M.R. Buckley and P.J. Fox, *Dark Matter Self-Interactions and Light Force Carriers*, *Phys. Rev. D* **81** (2010) 083522 [[arXiv:0911.3898](#)] [[INSPIRE](#)].
- [30] L.G. van den Aarssen, T. Bringmann and C. Pfrommer, *Is dark matter with long-range interactions a solution to all small-scale problems of Λ CDM cosmology?*, *Phys. Rev. Lett.* **109** (2012) 231301 [[arXiv:1205.5809](#)] [[INSPIRE](#)].
- [31] S. Tulin, H.-B. Yu and K.M. Zurek, *Resonant Dark Forces and Small Scale Structure*, *Phys. Rev. Lett.* **110** (2013) 111301 [[arXiv:1210.0900](#)] [[INSPIRE](#)].
- [32] S. Tulin, H.-B. Yu and K.M. Zurek, *Beyond Collisionless Dark Matter: Particle Physics Dynamics for Dark Matter Halo Structure*, *Phys. Rev. D* **87** (2013) 115007 [[arXiv:1302.3898](#)] [[INSPIRE](#)].
- [33] E. Del Nobile, M. Kaplinghat and H.-B. Yu, *Direct Detection Signatures of Self-Interacting Dark Matter with a Light Mediator*, *JCAP* **10** (2015) 055 [[arXiv:1507.04007](#)] [[INSPIRE](#)].
- [34] R. Foot and S. Vagnozzi, *Dissipative hidden sector dark matter*, *Phys. Rev. D* **91** (2015) 023512 [[arXiv:1409.7174](#)] [[INSPIRE](#)].
- [35] S.I. Blinnikov and M.Yu. Khlopov, *Possible astronomical effects of mirror particles*, *Sov. Astron. Zh.* **60** (1983) 632 [*Astron. Zh.* **27** (1983) 371] [[INSPIRE](#)].
- [36] M. Cirelli, M. Kadastik, M. Raidal and A. Strumia, *Model-independent implications of the e^\pm , \bar{p} cosmic ray spectra on properties of Dark Matter*, *Nucl. Phys. B* **813** (2009) 1 [*Addendum ibid.* **B 873** (2013) 530] [[arXiv:0809.2409](#)] [[INSPIRE](#)].
- [37] N. Arkani-Hamed, D.P. Finkbeiner, T.R. Slatyer and N. Weiner, *A Theory of Dark Matter*, *Phys. Rev. D* **79** (2009) 015014 [[arXiv:0810.0713](#)] [[INSPIRE](#)].
- [38] B. Bellazzini, M. Cliche and P. Tanedo, *Effective theory of self-interacting dark matter*, *Phys. Rev. D* **88** (2013) 083506 [[arXiv:1307.1129](#)] [[INSPIRE](#)].

- [39] F.-Y. Cyr-Racine and K. Sigurdson, *Cosmology of atomic dark matter*, *Phys. Rev. D* **87** (2013) 103515 [[arXiv:1209.5752](#)] [[INSPIRE](#)].
- [40] M. Kaplinghat, S. Tulin and H.-B. Yu, *Direct Detection Portals for Self-interacting Dark Matter*, *Phys. Rev. D* **89** (2014) 035009 [[arXiv:1310.7945](#)] [[INSPIRE](#)].
- [41] R. Laha and E. Braaten, *Direct detection of dark matter in universal bound states*, *Phys. Rev. D* **89** (2014) 103510 [[arXiv:1311.6386](#)] [[INSPIRE](#)].
- [42] XENON1T collaboration, E. Aprile, *The XENON1T Dark Matter Search Experiment*, *Springer Proc. Phys.* **148** (2013) 93 [[arXiv:1206.6288](#)] [[INSPIRE](#)].
- [43] SUPERCDMS collaboration, P.L. Brink, *Conceptual Design for SuperCDMS SNOLAB*, *J. Low. Temp. Phys.* **167** (2012) 1093 [[INSPIRE](#)].
- [44] J. Silk, K.A. Olive and M. Srednicki, *The Photino, the Sun and High-Energy Neutrinos*, *Phys. Rev. Lett.* **55** (1985) 257 [[INSPIRE](#)].
- [45] M. Srednicki, K.A. Olive and J. Silk, *High-Energy Neutrinos from the Sun and Cold Dark Matter*, *Nucl. Phys. B* **279** (1987) 804 [[INSPIRE](#)].
- [46] D.N. Spergel and W.H. Press, *Effect of hypothetical, weakly interacting, massive particles on energy transport in the solar interior*, *Astrophys. J.* **294** (1985) 663 [[INSPIRE](#)].
- [47] W.H. Press and D.N. Spergel, *Capture by the sun of a galactic population of weakly interacting massive particles*, *Astrophys. J.* **296** (1985) 679 [[INSPIRE](#)].
- [48] K. Griest and D. Seckel, *Cosmic Asymmetry, Neutrinos and the Sun*, *Nucl. Phys. B* **283** (1987) 681 [*Erratum ibid.* **B 296** (1988) 1034] [[INSPIRE](#)].
- [49] A. Gould, *WIMP Distribution in and Evaporation From the Sun*, *Astrophys. J.* **321** (1987) 560 [[INSPIRE](#)].
- [50] A. Gould, *Cosmological density of WIMPs from solar and terrestrial annihilations*, *Astrophys. J.* **388** (1992) 338 [[INSPIRE](#)].
- [51] A.R. Zentner, *High-Energy Neutrinos From Dark Matter Particle Self-Capture Within the Sun*, *Phys. Rev. D* **80** (2009) 063501 [[arXiv:0907.3448](#)] [[INSPIRE](#)].
- [52] I.F.M. Albuquerque, C. Pérez de Los Heros and D.S. Robertson, *Constraints on self interacting dark matter from IceCube results*, *JCAP* **02** (2014) 047 [[arXiv:1312.0797](#)] [[INSPIRE](#)].
- [53] C.-S. Chen, F.-F. Lee, G.-L. Lin and Y.-H. Lin, *Probing Dark Matter Self-Interaction in the Sun with IceCube-PINGU*, *JCAP* **10** (2014) 049 [[arXiv:1408.5471](#)] [[INSPIRE](#)].
- [54] ICECUBE collaboration, M.G. Aartsen et al., *Search for dark matter annihilations in the Sun with the 79-string IceCube detector*, *Phys. Rev. Lett.* **110** (2013) 131302 [[arXiv:1212.4097](#)] [[INSPIRE](#)].
- [55] DAMIC collaboration, J. Barreto et al., *Direct Search for Low Mass Dark Matter Particles with CCDs*, *Phys. Lett. B* **711** (2012) 264 [[arXiv:1105.5191](#)] [[INSPIRE](#)].
- [56] CRESST collaboration, G. Angloher et al., *Results on light dark matter particles with a low-threshold CRESST-II detector*, [arXiv:1509.01515](#) [[INSPIRE](#)].
- [57] SUPERCDMS collaboration, R. Agnese et al., *WIMP-Search Results from the Second CDMSlite Run*, submitted to *Phys. Rev. Lett.* (2015) [[arXiv:1509.02448](#)] [[INSPIRE](#)].
- [58] B. Holdom, *Two U(1)'s and Epsilon Charge Shifts*, *Phys. Lett. B* **166** (1986) 196 [[INSPIRE](#)].
- [59] E.C.G. Stueckelberg, *Interaction energy in electrodynamics and in the field theory of nuclear forces*, *Helv. Phys. Acta* **11** (1938) 225 [[INSPIRE](#)].
- [60] E.C.G. Stueckelberg, *Interaction forces in electrodynamics and in the field theory of nuclear forces*, *Helv. Phys. Acta* **11** (1938) 299 [[INSPIRE](#)].
- [61] N. Fornengo, P. Panci and M. Regis, *Long-Range Forces in Direct Dark Matter Searches*, *Phys. Rev. D* **84** (2011) 115002 [[arXiv:1108.4661](#)] [[INSPIRE](#)].

- [62] C.-S. Chen, G.-L. Lin and Y.-H. Lin, *Thermal transport of the solar captured dark matter and its impact on the indirect dark matter search*, [arXiv:1508.05263](#) [INSPIRE].
- [63] M.T. Frandsen, F. Kahlhoefer, S. Sarkar and K. Schmidt-Hoberg, *Direct detection of dark matter in models with a light Z'* , *JHEP* **09** (2011) 128 [[arXiv:1107.2118](#)] [INSPIRE].
- [64] J.L. Feng, J. Kumar and D. Sanford, *Xenophobic Dark Matter*, *Phys. Rev. D* **88** (2013) 015021 [[arXiv:1306.2315](#)] [INSPIRE].
- [65] J.D. Bjorken, R. Essig, P. Schuster and N. Toro, *New Fixed-Target Experiments to Search for Dark Gauge Forces*, *Phys. Rev. D* **80** (2009) 075018 [[arXiv:0906.0580](#)] [INSPIRE].
- [66] T. Lin, H.-B. Yu and K.M. Zurek, *On Symmetric and Asymmetric Light Dark Matter*, *Phys. Rev. D* **85** (2012) 063503 [[arXiv:1111.0293](#)] [INSPIRE].
- [67] J.L. Feng and J. Kumar, *The WIMPless Miracle: Dark-Matter Particles without Weak-Scale Masses or Weak Interactions*, *Phys. Rev. Lett.* **101** (2008) 231301 [[arXiv:0803.4196](#)] [INSPIRE].
- [68] LUX collaboration, D.S. Akerib et al., *First results from the LUX dark matter experiment at the Sanford Underground Research Facility*, *Phys. Rev. Lett.* **112** (2014) 091303 [[arXiv:1310.8214](#)] [INSPIRE].
- [69] J.L. Feng, J. Kumar, D. Marfatia and D. Sanford, *Isospin-Violating Dark Matter*, *Phys. Lett. B* **703** (2011) 124 [[arXiv:1102.4331](#)] [INSPIRE].
- [70] Y. Gao, J. Kumar and D. Marfatia, *Isospin-Violating Dark Matter in the Sun*, *Phys. Lett. B* **704** (2011) 534 [[arXiv:1108.0518](#)] [INSPIRE].
- [71] G.-L. Lin, Y.-H. Lin and F.-F. Lee, *Probing the coupling of heavy dark matter to nucleons by detecting neutrino signature from the Earth's core*, *Phys. Rev. D* **91** (2015) 033002 [[arXiv:1409.3094](#)] [INSPIRE].
- [72] PARTICLE DATA GROUP collaboration, K.A. Olive et al., *Review of Particle Physics*, *Chin. Phys. C* **38** (2014) 090001 [INSPIRE].
- [73] A. Baldini, V. Flamini, W.G. Moorhead, D.R.O. Morrison and H. Schopper, *Numerical Data And Functional Relationships In Science And Technology. Grp. 1: Nuclear And Particle Physics. Vol. 12: Total Cross-sections For Reactions Of High-energy Particles (including Elastic, Topological, Inclusive And Exclusive Reactions). Subvol*, Springer, Berlin Germany (1988) [INSPIRE].
- [74] B. Dasgupta and R. Laha, *Neutrinos in IceCube/KM3NeT as probes of Dark Matter Substructures in Galaxy Clusters*, *Phys. Rev. D* **86** (2012) 093001 [[arXiv:1206.1322](#)] [INSPIRE].
- [75] P. Baratella, M. Cirelli, A. Hektor, J. Pata, M. Piibeleht and A. Strumia, *PPPC 4 DM ν : a Poor Particle Physicist Cookbook for Neutrinos from Dark Matter annihilations in the Sun*, *JCAP* **03** (2014) 053 [[arXiv:1312.6408](#)] [INSPIRE].
- [76] ICECUBE collaboration, R. Abbasi et al., *The Design and Performance of IceCube DeepCore*, *Astropart. Phys.* **35** (2012) 615 [[arXiv:1109.6096](#)] [INSPIRE].
- [77] ICECUBE PINGU collaboration, M.G. Aartsen et al., *Letter of Intent: The Precision IceCube Next Generation Upgrade (PINGU)*, [arXiv:1401.2046](#) [INSPIRE].
- [78] M. Honda, T. Kajita, K. Kasahara, S. Midorikawa and T. Sanuki, *Calculation of atmospheric neutrino flux using the interaction model calibrated with atmospheric muon data*, *Phys. Rev. D* **75** (2007) 043006 [[astro-ph/0611418](#)] [INSPIRE].